

# 1 **Characterization of the Atlantic Water and Levantine Intermediate** 2 **Water in the Mediterranean Sea using 20 years of Argo Data**

3

4 Fedele Giusy<sup>1,\*</sup>, Mauri Elena<sup>1</sup>, Notarstefano Giulio<sup>1</sup> and Poulain Pierre Marie<sup>1</sup>

5

6 (1) National Institute of Oceanography and Applied Geophysics, OGS, 34010 Sgonico (TS), Italy

7 \* Corresponding author ([gfedele@inogs.it](mailto:gfedele@inogs.it))

8 The Atlantic Water (AW) and Levantine Intermediate Water (LIW) are important water  
9 masses that play a crucial role in the internal variability of the Mediterranean thermohaline  
10 circulation. In particular, their variability and interaction, along with other water masses that  
11 characterize the Mediterranean basin, such as the Western Mediterranean Deep Water (WMDW),  
12 contribute to modify the Mediterranean Outflow through the Gibraltar Strait and hence may  
13 influence the stability of the global thermohaline circulation.

14 This work aims to characterize the AW and LIW in the Mediterranean Sea, taking advantage  
15 of the large observational dataset provided by Argo floats from 2001 to 2019. Using different  
16 diagnostics, the AW and LIW were identified, highlighting the inter-basin variability and the  
17 strong zonal gradient that denote the two water masses in this marginal sea. Their temporal  
18 variability was also investigated in the last two-decades, providing a more robust view of the AW  
19 and LIW characteristics, which in previous studies, due to lack of data, have been investigated  
20 taking advantage of very short periods.

21 A clear salinification and warming trend characterize the AW and LIW in the last two decades  
22 ( $\sim 0.007 \pm 0.140$  and  $0.006 \pm 0.038$  yr<sup>-1</sup>;  $0.026 \pm 0.715$  and  $0.022 \pm 0.232$  °C yr<sup>-1</sup>, respectively). The  
23 salinity and temperature trends found at subbasin scale are in good agreement with previous  
24 results. The strongest trends are found in the Adriatic basin in both the AW and LIW properties.

25       **Keywords:** Argo, Atlantic Water, Interannual variability, Inter-basin variability, Levantine  
26 Intermediate Water, Mediterranean Sea, Trends

## 27       **Acknowledgments**

28       This research was funded by the Italian Ministry of University and Research as part of the Argo-  
29 Italy program.

30

## 31       **1 Introduction**

32       The Atlantic Water (AW) and Levantine Intermediate Water (LIW) play a central role in the  
33 internal variability of the Mediterranean thermohaline circulation, contributing to the dense water  
34 formation in this enclosed basin (Tsimplis et al., 2006). The variability and interaction of these  
35 two water masses modulate the Mediterranean outflow through the Gibraltar Strait, which plays  
36 an important role on the North Atlantic oceanic variability, and in turn to the stability of the global  
37 thermohaline circulation (e.g., Rahmstorf, 2006; Hernandez-Molina et al., 2014). Therefore, from  
38 a climatic point of view, it is relevant to characterize their main properties and monitor their  
39 variability, which are the main purpose of this paper.

40       Flowing in the Mediterranean Sea through the Gibraltar strait, the AW is less dense than the  
41 surrounding water masses and therefore it populates most of the Mediterranean surface layer. Its  
42 path is mainly driven by the Coriolis effect and by the complex topography that characterizes this  
43 region (Millot and Taupier-Letage 2005).

44       The LIW is the most voluminous water mass produced in the Mediterranean Sea (e.g., Skliris  
45 2014; Lascaratos et al., 1993), and the saltiest water formed with a relatively high temperature at  
46 intermediate depths. It is formed in the Levantine subbasin, after which it is named, where one of  
47 the main formation sites is the Rhodes Gyre (e.g., Tsimplis et al., 2006; Kubin et al., 2019). The  
48 LIW strongly influences the thermohaline circulation, flowing at intermediate depths and then  
49 passing over the sills, exiting the Gibraltar Strait and modifying the Atlantic circulation  
50 (Rahmstorf, 1998; Bethoux et al., 1999).

51 Several studies have been devoted to the analysis of the AW and LIW main features and  
52 variability, taking advantage of different indicators to identify and track these two water masses  
53 in the Mediterranean Sea. Among them, the AW and the LIW are usually referred to the minimum  
54 and maximum salinity in the surface and intermediate layers of the water column, respectively  
55 (e.g., Millot and Taupier-Letage 2005; Bergamasco and Malanotte-Rizzoli, 2010; Mauri et al.,  
56 2019; Juza et al., 2019; Kokkini et al., 2019; Vázquez-Yañez et al., 2020). However, different  
57 approaches can also be found in the literature. In particular Millot (2014) associated the LIW to  
58 the maximum of the potential temperature vertical gradient found in an intermediate water layer,  
59 while Bosse et al. (2015) identified the LIW in the northwestern Mediterranean Sea with the  
60 maximum salinity value found between two potential density values ( $\sigma_\theta = [29.03 - 29.10] \frac{kg}{m^3}$ ),  
61 encompassing both temperature and salinity maxima characterizing the LIW layer. The main  
62 findings related to the hydrological properties of these two water masses are summarized below.

63 The AW enters in the Mediterranean Sea through the Gibraltar Strait, occupying the upper 200  
64 m of depth with potential density, temperature and salinity annual mean values:  $\sigma_\theta \cong$   
65  $[26.5 - 27] \frac{kg}{m^3}$ ,  $T \cong [14 - 16]^\circ C$ ,  $S \cong [36.0 - 36.5]$  respectively (e.g., Bergamasco and  
66 Malanotte-Rizzoli, 2010; Hayes et al., 2019). The AW flowing at the surface, continuously  
67 interacts with the atmosphere and is subject to evaporation and mixing with the underlying water  
68 masses. Flowing eastward, it becomes denser and the minimum salinity core sinks. Therefore, it  
69 can be capped by the surface mixed layer and less influenced by air-sea interactions. Its properties  
70 and variability are also modified by the local eddies and by the river discharges in the coastal  
71 regions. These mechanisms shape the AW, leading to an increase of salinity from about 36.25 in  
72 the Gibraltar Strait to values around 39.2 in the Levantine Sea (e.g., Bergamasco and Malanotte-  
73 Rizzoli, 2010; Hayes et al., 2019). These values highlight strong AW temperature and salinity  
74 gradients between the Western Mediterranean (WMED) and the Eastern Mediterranean (EMED).

75 The properties of the LIW core in the WMED are commonly referred to the following ranges  
76 of potential density, temperature, salinity and depth, respectively:  $\sigma_\theta = [29 - 29.10] \frac{kg}{m^3}$ ,  $T =$   
77  $[13 - 14.2]^\circ C$ ,  $S = [38.4 - 38.8]$ ,  $D = [200 - 600]m$  (e.g. Millot, 2013; Hayes et al., 2019;

78 Várgas-Yañez et al., 2020); while in the EMED these properties span over different values:  $\sigma_{\theta} =$   
79  $[28.85 - 29.15] \frac{kg}{m^3}$ ,  $T = [14.6 - 16.4]^{\circ}C$ ,  $S = [38.85 - 39.15]$ ,  $D = [150 - 400]m$  (e.g.  
80 Lascaratos et al., 1993; Hayes et al., 2019). Therefore, moving westward,  $T$  and  $S$  decrease and  
81 the LIW sinks.

82 These studies provide a general view of the AW and LIW properties in the Mediterranean Sea,  
83 highlighting a strong inter-basin variability of these water masses along their paths, which in turn  
84 influences their temporal changes.

85 An example is given by a recent paper by Kassis and Korres (2020), which provides a detailed  
86 view of the EMED hydrographic properties for the period 2004–2017 taking advantage of Argo  
87 data. Exploring the water column from the surface down to 1500 m in seven different regions of  
88 the EMED, they revealed a high inter-annual variability of the stored heat and salt over this region.

89 In this study, following a similar approach, we investigate the AW and LIW properties,  
90 isolating their main characteristics and variability from the surrounding water masses, taking  
91 advantage of several diagnostics discussed in section 2.2. Our work aims to provide a more robust  
92 view of the AW and LIW characteristics, which in previous studies, due to lack of data, have been  
93 investigated taking advantage of short periods.

94 In the frame of climate change studies, it is important to estimate possible impacts of AW and  
95 LIW changes on the Mediterranean climate, since this region is one of the most vulnerable climate  
96 change hotspots (Giorgi 2006). In fact, changes in temperature and salinity can strongly affect the  
97 marine system over the Mediterranean and related human activities.

98 Previous studies highlighted a clear salinification of the Mediterranean Sea over the past few  
99 decades (e.g., Painter and Tsimplis 2003; Vargas -Yañez et al., 2010; Schroeder et al., 2017;  
100 Skliris et al., 2018) and a clear deep water warming trend after 1980s, which in literature is often  
101 related to the Nile River damming and to the global warming (Vargas-Yañez et al., 2010). Positive  
102 temperature and salinity trends, oscillating between  $[0.0016 \div 0.0091]^{\circ}C/yr$  and  $[0.0008 \div 0.001]$   
103  $yr^{-1}$ , respectively, are found in the deep layer (below  $\sim 700$  meters) between 1950 to 2005 (e.g.,  
104 Bethoux et al., 1990; Rohling and Bryden, 1992; Millot et al., 2006; Vargas-Yañez et al., 2010;  
105 Borghini et al., 2014).

106 This observed salinification and warming are also found at intermediate depths in several  
107 studies (e.g., Zu et al., 2014; Schroeder et al., 2017; Skliris et al., 2018), with ranges that depend  
108 on the region of investigation. A clear positive salinity trend between 150-600 m is found in the  
109 Mediterranean Sea by Skliris et al. (2018), analyzing the MEDATLAS data from 1950 to 2002  
110 ( $\sim 0.007 \pm 0.004 \text{ yr}^{-1}$ ).

111 In contrast, heterogeneous temperature trends are found in the upper layer in different regions  
112 (Painter and Tsimplis, 2003). This sensitivity of the trends to the area of interest, can be due to  
113 several reasons, such as the changes in the large-scale atmospheric forcing of the Mediterranean  
114 region, the river runoff which differ from one region to another, and to the data coverage over a  
115 specific area (e.g., Painter and Tsimplis, 2003; Vargas -Yáñez et al., 2009; 2010). In this respect,  
116 Vargas -Yáñez et al. (2009) highlighted that the scarcity of data makes trend estimations very  
117 sensitive to the data postprocessing, comparing results from different studies dealing with the  
118 same time period. Therefore, in order to reduce the uncertainty of the trend estimations, longer  
119 and less sparse timeseries are needed.

120 In this respect, this work aims to provide an updated view of the temporal evolution and trends  
121 of the AW and LIW, taking advantage of the large observational dataset provided by the MedArgo  
122 Program (Poulain et al., 2007). It covers the water column from the surface down to  $\sim 2000$  m  
123 over the entire Mediterranean basin from 2001 to 2019. The Mediterranean Sea has been widely  
124 studied through the deployment of hundreds of Argo profiling floats (Argo 2020) in the last two  
125 decades as part of various national, European and international programs (Wong et al., 2021) and  
126 with the participation of different institutions. For these reasons, this dataset constitutes an optimal  
127 observational framework to investigate the AW and LIW properties.

128 The dataset and the methods used in this study are described in section 2, the results are  
129 presented in section 3, where the inter-basin and inter-annual variabilities of the AW and LIW in  
130 the Mediterranean Sea are shown. The main conclusions are drawn in section 4.

131

## 132 **2 Data and method**

### 133 **2.1 Data**

134 In this work the AW and LIW properties in the Mediterranean Sea are investigated taking  
135 advantage of the Argo float dataset, which consists of more than thirty thousand *T-S* profiles for  
136 the period 2001–2019. Since 2001, the number of observations is generally increasing, reaching  
137 a peak of 4188 profiles in 2015, mainly thanks to the combined efforts of national and  
138 international Argo initiatives. The deployments of most Argo floats in the Mediterranean were  
139 coordinated by the MedArgo regional center (Poulain et al., 2007). In the Mediterranean, the  
140 cycling period is usually reduced to 5 days, and the maximum profiling depth is mostly 700 or  
141 2000 m (Poulain et al., 2007). The floats are equipped with Sea-Bird Conductivity-Temperature-  
142 Depth (CTD) sensors (model SBE41CP; [www.seabird.com/sbe-41-argo-ctd/product-](http://www.seabird.com/sbe-41-argo-ctd/product-details?id=54627907875)  
143 [details?id=54627907875](http://www.seabird.com/sbe-41-argo-ctd/product-details?id=54627907875)) with accuracies of  $\pm 0.002^\circ\text{C}$ ,  $\pm 0.002$  and  $\pm 2$  dbar for temperature,  
144 salinity and pressure, respectively. The data measured by the profilers are transmitted to satellites  
145 (e.g., via the Iridium or Argos telemetry systems), then to ground receiving stations, processed  
146 and real-time quality-controlled by the Argo Data Assembly Centres ([https://www.euro-](https://www.euro-argo.eu/Activities/Data-Management/Euro-Argo-Data-Centres)  
147 [argo.eu/Activities/Data-Management/Euro-Argo-Data-Centres](https://www.euro-argo.eu/Activities/Data-Management/Euro-Argo-Data-Centres)), sent to the Global Data  
148 Assembly Center and made available for free to users ([https://fleetmonitoring.euro-](https://fleetmonitoring.euro-argo.eu/dashboard?Status=Active)  
149 [argo.eu/dashboard?Status=Active](https://fleetmonitoring.euro-argo.eu/dashboard?Status=Active)). The delayed-mode quality control applied on pressure,  
150 temperature and salinity follows the guidelines described in the Argo Quality Control Manual for  
151 CTD (e.g., Wong et al., 2021; Cabanes et al., 2016), in conjunction with other procedures  
152 developed at regional level (Notarstefano and Poulain, 2008; Notarstefano and Poulain, 2013) to  
153 check the salinity data and any potential drift of the conductivity sensor.

154 The analyses are performed in eight Mediterranean sub-basins following the climatological  
155 areas defined by the EU/MEDARMEDATLAS II project  
156 (<http://nettuno.ogs.trieste.it/medar/climatologies/medz.html>), emphasizing the processes that take  
157 place in each sub-basin and modify the water mass properties. Fig. 1 shows the geographical  
158 distribution of the Argo profiles from 2001 to 2019 in the eight sub-basins considered (Algerian,  
159 Catalan, Ligurian, Tyrrhenian, Adriatic, Ionian, Cretan and Levantine). The Alboran, Aegean and  
160 the Sicily Channel sub-basins are not analyzed in this work due to the scarcity of observations in  
161 these areas.

162 Most sub-basins are well spatially covered, except for the Adriatic Sea, where the majority of  
163 observations are concentrated in the South Adriatic Pit (SAP) and therefore it is important to keep  
164 in mind that the results found for this region, are representative of the southern Adriatic Sea. The  
165 SAP is an important deep water convection site in the Mediterranean Sea (e.g., Kokkini et al.,  
166 2019; Mauri et al., 2021; [Mihanović et al. \(2021\)](#); Azzaro et al., 2012; Bensi et al., 2013) and  
167 therefore it is also considered as a crucial area from a climatic perspective. The temporal  
168 distribution of the float data is different in the various sub-basins: the longest time series are  
169 available in the Ionian, Cretan and Levantine regions, with data from 2001 to 2019, followed by  
170 the Algerian, Ligurian and Tyrrhenian sub-basins where data are available after 2003, and then  
171 by the Adriatic Sea with data only after 2009. In this context, it is important to mention that the  
172 low density in space and time of the Argo profiles induces uncertainties in the results, especially  
173 during the first years of the analyzed period.

174

## 175 **2.2 Methods**

176 As discussed in the introduction, many indicators/characteristics have been adopted in  
177 literature to track the AW and LIW in the Mediterranean Sea. Most of them consider, as best  
178 indicator, the minimum/maximum salinity at surface/intermediate layer for the AW/LIW and  
179 motivated us to follow a similar approach (e.g., Millot and Taupier-Letage, 2005; Bergamasco  
180 and Malanotte-Rizzoli, 2010; Hayes et al., 2019; Lamer et al., 2019).

181 A preliminary step in this analysis was the post-processing: we first applied a time sub-  
182 sampling on each profiler to obtain a more homogeneous dataset (Notarstefano and Poulain,  
183 2009). This is applied to each float as follows: if the cycling period is 1 day or less, the profiles  
184 are sub-sampled every 5 days; if the period is 2 or 3 days, they are sub-sampled every 6 days; and  
185 if the period is 5 or 10 days, no subsampling is applied. Afterward, each profile was linearly  
186 interpolated from the surface (0 m) to the bottom every 10 m to obtain comparable profiles; and  
187 finally, a running filter with a 20 m window, was applied to the data along the depth axis, to  
188 smooth any residual spike.

189 Finally, the minimum/maximum salinity value in each profile is associated to the AW/LIW  
190 core in the respective depth layer. Then, the correspondent depth and temperature values are  
191 considered.

192 Once the AW and LIW core are identified in each profile, the AW and LIW inter-basin  
193 variabilities were analyzed taking advantage of the boxplot approach applied to each parameter  
194 and region (Fig. 2). In Fig.2, the whiskers (black dashed line out of the box) extend to the most  
195 extreme data points not considering the outliers at the 5% significance level ( $pvalue \leq 0.05$ ). In  
196 order to test the significance, the Student's  $t$  distribution was applied to each hydrological  
197 parameter in every sub-basin (Kreyszig and Erwin 1970). The null hypothesis (that states that the  
198 population is normally distributed) is rejected with a 5% level of statistical significance. This  
199 method is also applied to the timeseries trends. In section 3.1 we often refer to the range and  
200 skewness of the distributions, that are the difference between the upper and lower limits and the  
201 measure of the symmetry of the distributions, respectively (including only the 5% significance  
202 values).

203 Considering only the AW/LIW salinity, temperature, and depth values at 95% level of  
204 significance (Fig.2), as done for the spatial analysis, the timeseries from 2001 to 2019 have been  
205 computed in each subbasin to analyze the low frequency variability (LFV) and trends at  
206 interannual to decadal timescale over the available observed periods. In this respect, the high  
207 frequency variability was filtered out, first by subtracting the mean seasonal cycle to the raw  
208 timeseries, and then applying a median yearly average filter. This last step is needed since the  
209 data are not homogeneous in time in every subbasin from 2001 to 2019, and therefore without it,  
210 the seasonal variability can contaminate the estimation of the trends. The latter have been  
211 computed using the linear least-squares method to fit a linear regression model to the data.

212

### 213 **3 Results and discussion**

214 In this section, the AW and LIW properties are investigated in the eight Mediterranean climatic  
215 regions before mentioned, focusing both on their spatial and temporal variability. The analysis of  
216 the trends and spectral features are also shown.



217

### 218 **3.1 Inter-basin variability**

#### 219 (i) AW

220 The hydrological properties of the AW core in eight sub-basins (Fig. 1) are shown in Figs. 2a,  
221 b, c, providing a compact view of the AW inter-basin variability for each parameter using the  
222 boxplot approach.

223 Moving eastward, the AW salinity increases from  $\sim 36$  to  $39.5$  (minimum and maximum  
224 whiskers limits; Fig. 2a), since the surface salinity minimum is progressively smoothed by  
225 horizontal mixing with surrounding saltier waters. In fact, as discussed by Font et al. (1998) the  
226 AW minimum salinity is dependent on the different degrees of mixing due to its residence times.

227 In the Algerian sub-basin, the salinity range reaches the highest extension compared to the  
228 other regions, probably due to the large baroclinic instability that produces high mesoscale  
229 variability in the surface layer and horizontal mixing by strong eddies (Demirov and Pinardi  
230 2007).

231 The AW salinity range is smaller in the Catalan, Ligurian and Tyrrhenian Seas, where similar  
232 distributions are found both in terms of range and skewness (which is close to zero): the main  
233 mode and the median have salinity of  $\sim 38$ . In the Adriatic Sea the distribution is probably skewed  
234 toward higher values because a clear positive salinity trend is found (Fig. 3; Lipizer et al., 2014).  
235 In the Adriatic, Ionian and Cretan Seas, the range is higher than the surrounding sub-basins: in  
236 the Adriatic and Ionian Sea this could be associated to the Bimodal Oscillation System (BiOS),  
237 and then to the reversal of the North Ionian Gyre (Rubino et al., 2020), while in the Cretan Sea  
238 we speculate that it is caused by the sinking of the AW during winter. This is in agreement with  
239 Schroeder (2019), where it is shown that in the Cretan Sea, the strong wind-induced evaporation  
240 and heat loss during winter lead the AW transformation into salty and warm Cretan Intermediate  
241 Water. The depths reached in the Cretan basin (Fig. 2c) seem to confirm this hypothesis.

242 The AW temperature is highly variable, ranging between  $\sim 5$  and  $\sim 30$  °C, with a wider range  
243 in the Catalan and Adriatic regions (Fig. 2b), possibly due to the higher seasonal sea surface  
244 temperature variability over these sub-basins (Shaltout and Omstedt 2014). The lowest

245 temperatures detected can be related to the freshwater fluxes in these regions. In this respect, an  
246 episode that can be relevant for the AW distribution in the Adriatic Sea is the large river runoff  
247 observed in 2014 by Kokkini et al. (2019), which caused a saline stratification for more than a  
248 year. This episode is also captured by our analyses (Fig. 3). As observed for the AW salinity  
249 mode, even the temperature mode shift toward higher values moving eastward in agreement with  
250 the literature (Bergamasco and Malanotte-Rizzoli 2010). In the Algerian basin the AW  
251 temperature mode is higher than it is in the Catalan subbasin: this can be due to the influence of  
252 freshwater fluxes in the Catalan region and led by the high eddy activity over the Algerian region  
253 (Escudier et al., 2016) led by the strong baroclinic instability already discussed for the salinity  
254 field (e.g., Demirov and Pinardi 2007; Cotroneo et al., 2016; Aulicino et al., 2018; Aulicino et al.,  
255 2019). The temperature and salinity ranges captured in the Algerian region are in good agreement  
256 with those found by Cotroneo et al. (2020) and shown in their Table 2.

257 The depths of the AW core oscillate between 0 and 90 m with the main mode sinking eastward  
258 (Fig. 2c). The distributions are all skewed toward lower depths, with the maximum probability  
259 density function (PDF) near surface and a median shifting from 0 to 45 m moving eastward,  
260 indicating a clear sinking of the AW along its pathway.

261

## 262 (ii) LIW

263 In this section, the main hydrological properties of the LIW are analyzed in each sub-basin.

264 Flowing away from the region of formation, the LIW interacts with the surrounding water  
265 masses and becomes less salty; the salinity sharply drops from  $\sim 39.2$  to  $\sim 38.5$ , moving from the  
266 Levantine to the Ligurian subbasin, and then it becomes more stable in the Algerian and Catalan  
267 regions, oscillating around  $\sim 38.5$  (Fig. 2e). The distributions are highly symmetric around the  
268 median and the variability decreases flowing westward maybe because the LIW becomes deeper,  
269 sinking from  $\sim 100$  to  $\sim 650$  m (Fig. 2g). The highest salinity is reached in the Cretan basin, where  
270 the formation of salty and warm Cretan Intermediate Water, caused by strong wind-induced  
271 evaporation and heat loss during winter, influences the LIW properties and detection (Schroeder,  
272 2019).

273 The LIW temperature decreases westward from ~18 to ~12.8 °C. The range is higher in the  
274 EMED as also found for salinity, suggesting that over this region, the intrusion of warmer and  
275 saltier surface waters due to convective processes characterizes the LIW formation (Fig. 2f;  
276 Schroeder, 2019).

277 The sinking of the LIW flowing westward is shown in Fig. 2g, dropping from about 100 to  
278 650 m (maximum whiskers values). The distributions tend to be symmetric in most of the  
279 Mediterranean Sea, except for the Adriatic Sea, where a strong LIW bimodality in the depth  
280 domain is found, with two peaks located at ~190 and ~500 m respectively (here not shown), in  
281 agreement with Kokkini et al. (2019) and Mihanović et al. (2021). In this respect, Mihanović et  
282 al. (2021), analyzing observed data from CTD measurements, Argo floats, several glider  
283 missions, satellite observations and operational ocean numerical model products, provides a  
284 possible explanation to this double-maxima vertical pattern, suggesting that these two peaks may  
285 be explained by two concurrent events: the winter convection at the beginning of 2017, which  
286 leads higher salinities in the water column, and a very strong inflow of high salinity waters from  
287 the Northern Ionian in late winter and spring of 2017, which this time is restricted almost to the  
288 surface.

289

## 290 **3.2 Interannual variability**

291 In this section, the temporal variability of the AW and LIW in each sub-basin is studied  
292 analyzing the 1-year moving average timeseries and the relative trends.

293 The results of this analysis are affected by the irregular spatial and temporal sampling of the  
294 Argo floats. Time gaps in the data are found in the Catalan, Tyrrhenian and Cretan Seas (Fig. 3).  
295 The missing data are due to the lack of Argo float samplings. Data in the Adriatic Sea are available  
296 only after 2009, while the Ionian, Cretan and Levantine sub-basins have much longer timeseries,  
297 with data covering the period from 2001 to 2019.

298

### 299 **3.2.1 Trends**

300 (i) AW trends

301 The AW salinity temporal evolution is shown in Fig. 3, where significant trends (at 5% level of  
302 significance) are found in each region (Table 1). Positive trends are clearly found in the EMED  
303 and in the Tyrrhenian Sea, highlighting a clear salinification of the AW in the last two decades  
304 over most of the Mediterranean Sea ( $\sim 0.007 \pm 0.140 \text{ yr}^{-1}$ ; Table 1). Comparable positive salinity  
305 trends between 0-150 m ( $\sim 0.009 \pm 0.009 \text{ yr}^{-1}$ ) are also found in Skliris et al. (2018) where multi-  
306 decadal salinity changes in the Mediterranean Sea are investigated taking advantage of the  
307 MEDATLAS database (MEDAR Group 2002) consisting of temperature and salinity profiles in  
308 the Mediterranean from 1945 to 2002  
309 (<https://www.bodc.ac.uk/resources/inventories/edmed/report/4651/>). A clear meridional  
310 separation is found in the AW trends during the observed period. In the Tyrrhenian Sea and in the  
311 entire EMED the AW becomes saltier, with significant positive trends, whilst in the WMED, a  
312 significant negative trend emerges in the Algerian and Catalan subbasins (Table 1). This  
313 freshening of the AW inflow could be related to the observed rapid freshening of the North  
314 Atlantic Ocean (Dickson et al. 2002), which causes are related to different phenomenon, included  
315 the accelerating Greenland melting triggered by the global warming (Dukhovskoy et al., 2019).  
316 These findings seem in contradiction with the results provided by Millot (2007), showing a  
317 salinification of the Mediterranean outflow, obtained analyzing autonomous CTDs on the  
318 Moroccan shelf in the strait of Gibraltar in the period 2003-2007, which may be caused by the  
319 different epochs under study. In fact, comparing Fig. 3 in Millot (2007) and Fig. 3 in this work, a  
320 similar positive trend is captured in the Algerian sub-basin, in the same period; while extending  
321 the analysis to a longer timeseries, a clear negative trend leads the AW variability at interannual  
322 to decadal timescale. Opposite trends are found in the EMED and in the Tyrrhenian subbasin,  
323 where the very strong increase in net evaporation of  $\sim 8$  to 12% over 1950-2010 (Skliris et al.,  
324 2018) and the damming of the Nile River (as projected by Nof, 1979) may have caused the AW  
325 salinification. The trends are steep in the Adriatic and Cretan sub-basins, where the salinity  
326 increases with an order of magnitude higher ( $O[10^{-2}]$ ) and the largest increase is found in the  
327 Adriatic Sea ( $0.044 \pm 0.188 \text{ yr}^{-1}$ ). Here the impact of the negative E-P anomalies and large river  
328 runoff observed by Kokkini et al. (2019) around 2014 is well captured by the salinity time series.

329 The results in the EMED are in good agreement with Fig. 9 of Kassis and Korres (2020), where  
330 the yearly average salinity per depth zone and per region between 2004-2017 are shown.  
331 Similarities in the observed trend in the Ionian Sea ( $0.009 \pm 0.181 \text{ yr}^{-1}$ ) are also found by Zu  
332 et al., 2014 (mean trend  $\sim 0.011 \text{ yr}^{-1}$ ), where the Argo floats data between 2004 and 2014 are  
333 analyzed.

334 According to the above-mentioned meridional salinity transition from negative to positive  
335 salinity trends moving eastward, the temperatures also show a meridional shift from positive to  
336 negative significant trends east of the Ionian Sea, with a mean positive AW temperature trend  
337 over the eight analyzed sub-basins ( $0.026 \pm 0.715 \text{ }^\circ\text{C/yr}$ ; Table 1). Interbasin changes between  
338 the subbasins are instead linked to changes in the large-scale meteorological forcing of the  
339 Mediterranean region (Painter and Tsimplis, 2003). As found for the salinity field, the sharper  
340 increase is related to the Adriatic Sea ( $\sim 0.117 \pm 0.951 \text{ }^\circ\text{C/year}$ ), highlighting the presence of  
341 mechanisms that enhance the trends over this region. A sharpening in the trend over the last  
342 decade is captured in the Catalan subbasin (Fig.7) and confirmed by Schuckmann et al. (2019),  
343 who observed the same behavior in the Northwestern Mediterranean with a trend over the last  
344 decade ( $\sim 0.047 \text{ }^\circ\text{C/yr}$ ), that doubles the respective trend in the previous 1982-2011 period ( $0.029$   
345  $^\circ\text{C/yr}$ ).

346 The AW depths time series (Fig. 5) show a heterogeneous trend in the Mediterranean Sea,  
347 with significant negative values (the depth decreases) in the Algerian and Ionian subbasins, and  
348 positive in the Tyrrhenian and Levantine regions (Table 1), which reflects into a tendency of the  
349 AW to become shallower, increasing the stratification at basin scale ( $0.238 \pm 10.537 \text{ m/yr}$ ). Wider  
350 temporal changes are found in the Levantine region, where the trend is from one to two orders of  
351 magnitude higher than the other regions.

352

## 353 (ii) LIW

354 The LIW temporal variability is hereafter analyzed. Fig. 6 shows the salinity changes from  
355 2001 to 2019 in the eight subbasins considered. A positive trend is found in the whole

356 Mediterranean Sea at 5% level of significance, highlighting a salinification also at intermediate  
357 depths of this enclosed basin over two decades ( $\sim 0.006 \pm 0.038 \text{ yr}^{-1}$ ; Table 1). A similar positive  
358 trend between 150-600 m is found by Skliris et al. (2018), in the MEDATLAS data from 1950 to  
359 2002 ( $\sim 0.007 \pm 0.004 \text{ yr}^{-1}$ ), with lower standard deviations. The higher standard deviations found  
360 in this study, compared to those founds by Skliris et al. (2018) could be related to the wider range  
361 of depths considered and to the different epochs considered. The LIW properties vary less than  
362 the AW in most of the basin, except for the Ligurian, and Levantine regions, where deep water  
363 and LIW water formations occur respectively. The strongest salinity increase is found in the  
364 Adriatic Sea ( $0.021 \pm 0.074 \text{ yr}^{-1}$ ), exceeding the trends in other regions by one order of magnitude.  
365 The Adriatic salinity trend from 2008 to 2018 is about five times larger than the Adriatic salinity  
366 trend observed in the period 1952-2010 and quantified by Vilibić et al. (2013). The possible  
367 source of such a large trend, may come by the biasing of the signal by the BiOS oscillations, since  
368 the series starts in 2008, when the anticyclonic BiOS was present. Here, the periodicity of the  
369 BiOS has a magnitude which is comparable with the timeseries length in the Adriatic, which  
370 might be also relevant for other sub-regions. Therefore, longest timeseries are needed to better  
371 estimate the trend over this sub-basin.

372 The LIW salinity positive trends over the Mediterranean Sea are also found by Zu et al. (2014),  
373 which confirms the salinification of the basin at intermediate depths, as also observed at surface  
374 in most of the analyzed regions. This suggests that the enhancement of the net evaporation over  
375 the Mediterranean in the last decades, that was observed by Skliris et al. (2018), may lead the  
376 formation of saltier LIW in the EMED, and as consequence a mean positive salinity trend over  
377 the whole basin. While, in the WMED, positive trends ( $0.008 \pm 0.002$ ;  $0.009 \pm 0.0007 \text{ yr}^{-1}$ ; from  
378 gliders missions) are found from 2011 to 2017 by Juza et al. (2019), in agreement with the positive  
379 trends found in the last few years in the western subbasins shown in Fig.6.

380 Positive temperature trends (5% level of significance) are found in the whole Mediterranean  
381 Sea except in the Levantine sub-basin, where the negative trend could be related to oscillations  
382 with decadal timescales that take place over this region. This is confirmed by the continuous  
383 wavelet transforms applied to the timeseries (not shown). Peaks of salinity and temperature are

384 observed in ~2009 in the Levantine basin and then reach the Cretan Sea in ~2010. The same  
385 variability is discussed in Ozer et al. (2017) and explained in connection with the Ionian Bimodal  
386 Oscillating System (BiOS). These maxima are in fact attributed to periods of anticyclonic  
387 circulation in the north Ionian (2006-2009) and limited AW advection to the south-eastern  
388 Levantine basin, referring to the study by Artale et al. (2006). The LIW temperature mean trend  
389 and standard deviation averaged over the eight subbasins are  $\sim 0.002 \pm 0.232$  °C/yr (Table 1),  
390 which can be interpreted as a weaker response of the intermediate layers to the warming trend  
391 observed at surface.

392 The sub-basins with the steepest increase are located in the central longitudinal band of the  
393 Mediterranean Sea, therefore far from the LIW main sources. The range of temperature and  
394 salinity and the respective variability in the Tyrrhenian and Ionian sub-basins are in good  
395 agreement with Poulain et al. (2009), where  $T$  and  $S$  timeseries from 2001 to 2009 are computed  
396 from Argo floats data near 600 m. The ranges and trends for  $T$  and  $S$  found in the Ligurian Sea  
397 are also confirmed by Margirier et al. (2020), where vertical profiles collected by gliders, Argo  
398 floats, CTDs and XBTs in the northwestern Mediterranean Sea over the 2007–2017 period are  
399 analyzed.

400 The LIW depth time series are shown in Fig. 8: significant negative trends (the depth  
401 decreases) are found in the Tyrrhenian, Ionian, and Cretan Seas, while in the Catalan and  
402 Levantine sub-basins the LIW sinks ( $pvalue \leq 0.05$ ). Non-significant trends are found in the  
403 other regions. Abrupt shifts are found in the Adriatic sub-basin from ~200 m to ~500-600 m at  
404 different time steps (trend  $\sim 2.609 \pm 115.404$  m/yr), highlighting a bimodal behavior of the LIW  
405 depth and an intense dense water production activity as also shown by Kokkini et al. (2019) and  
406 Mihanović et al. (2021). Previous studies attribute dramatic shifts in the Adriatic hydrological  
407 properties to the BiOS and the Eastern Mediterranean Transient (e.g., Vilibić et al., 2012). This  
408 hypothesis can also be supported by correlations between the BiOS (definition by Vilibić et al.,  
409 2020) and the AW/LIW salinity yearly averaged timeseries in the Adriatic Sea, which maximum  
410 values are about -0.49/-0.43 at lag 0 /-4 yr (at negative year lag, the BiOS leads;  $pvalue \leq 0.05$ ).  
411 Further investigations are left to future studies.

412 The results related to the EMED match those shown in Kassis and Korres (2020), where the  
413 timeseries of salinity and temperature averaged between different depths-layers (below 100 m) in  
414 similar subbasins are shown (see Fig. 8 in Kassis and Korres 2020). The LIW depth mean trend  
415 and standard deviation averaged over the eight subbasins is  $1.099 \pm 46.458$  m/yr (Table 1).

416

#### 417 **4 Conclusions**

418 We presented an analysis of the main properties and variability of the AW and LIW in the  
419 Mediterranean Sea, exploiting the Argo float data that provide an optimal observational dataset  
420 to study their thermohaline properties. Indeed, this dataset covers the water column down to  
421 ~2000 m and provide data for almost two decades.

422 Taking advantage of different diagnostics discussed in section 2, the AW and LIW have been  
423 detected in the Mediterranean Sea through a sub-basin approach, which allowed to define the  
424 main hydrological features over this enclosed basin in different regions.

425 In addition to previous studies, this work provides a more detailed view of the AW and LIW  
426 characteristics in the last two-decades over most of the Mediterranean Sea, except for the Alboran  
427 sub-basin, the Sicily Channel, and the Aegean sub-basin where Argo data are too scarce.

428 To achieve this goal, the first step of this study was the detection of the AW and LIW cores in  
429 each available profile. In agreement with previous studies (e.g., Lascaratos et al., 1993;  
430 Bergamasco and Malanotte-Rizzoli, 2010; Millot, 2013; Hayes et al., 2019; Vargas-Yanez et al.,  
431 2020), we confirmed the mean zonal gradients of the AW and LIW properties over the  
432 Mediterranean Sea: the AW becomes saltier, warmer, and deeper moving eastward, while the  
433 LIW becomes fresher, colder, and deeper moving westward. These results not only match the  
434 present literature but also provide a more detailed view of these water masses over eight sub-  
435 basins.

436 The timeseries derived from the AW and LIW parameters have also highlighted some  
437 interesting features that are in good agreement with the previous literature. The most relevant  
438 results are summarized below:



- 439
- Positive salinity and temperature trends characterize the AW and LIW in the last two  
440 decades over most of the Mediterranean Sea (average value over the whole region:  
441 0.007 and 0.006 yr<sup>-1</sup>; 0.026 and 0.022 °C/yr respectively). The warming and  
442 salinification of the Mediterranean Sea is in good agreement with previous results  
443 (e.g., Skliris et al., 2018; Margirier et al., 2020; Kassis and Korres, 2020).
  - Negative AW salinity trends in the Algerian and Catalan sub-basins suggest a  
444 freshening of the AW inflow, in agreement with the observed rapid freshening of the  
445 North Atlantic Ocean (Dickson et al., 2002).
  - Positive AW salinity trends are found east of the Ligurian sub-basin, highlighting a  
446 clear salinification of this water mass in the last two decades probably due to the  
447 combined effect of the strong increase in net evaporation and the Nile dummung (e.g.,  
448 Nof, 1979; Skiliris et al., 2018; section 3.2.1a).
  - Positive trends in the LIW salinity timeseries are found in the whole Mediterranean  
449 Sea at 5% level of significance, highlighting a salinification also at intermediate  
450 depths (section 3.2.1b).
  - Positive LIW temperature trends (*pvalue* ≤ 0.05) are found everywhere except in the  
451 Levantine sub-basin, where the negative trend might be related to oscillations with  
452 decadal timescales, that play a role in this region. These results highlight a clear  
453 warming at intermediate depth in most of the Mediterranean Sea.
  - The AW and LIW depth trends are highly space-dependent, showing different  
454 behaviors in the eight sub-basins.
  - Abrupt shifts in the LIW depth are found in the Adriatic sub-basin from ~200 m to  
455 ~500-600 m at different time steps (trend 2.609±115.404 m/yr), highlighting a  
456 bimodal behavior of the LIW depth and an intense dense water production activity as  
457 also shown by Kokkini et al. (2019) and Mihanović et al. (2021).
  - The timeseries length could affect the measure of the trends in the sub-basins that are  
458 interested by forcings with periodicity with the same order of magnitude. In this  
459

466            respect, the trends observed in the Adriatic Sea are clearly impacted by the BiOS,  
467            since the timeseries starts in 2008, when the anticyclonic BiOS was present. This  
468            might be also relevant for other sub-regions.

469            These results therefore provide interesting new insights about the AW and LIW interbasin and  
470            interannual variability, that can be further analyzed to investigate which mechanisms lead to the  
471            observed temporal trends in each sub-basin.

472       **References**

473

474    Argo: Argo float data and metadata from Global Data Assembly Centre (Argo GDAC). SEANOE.  
475       <https://doi.org/10.17882/42182>, 2020.

476

477    Artale V., Calmante S., Malanotte-Rizzoli P., Pisacane G., Rupolo V., and Tsimplis M., In: Li-  
478       onello, P., Malanotte-Rizzoli, P., Boscoli, R. (Eds.), *The Atlantic and Mediterranean Sea as*  
479       *connected systems*, in *Mediterranean Climate Variability Dev. Earth Environ. Sci. 4*. Else-  
480       vier, Amsterdam, pp. 283–323, 2006.

481

482    Aulicino G., Cotroneo Y., Ruiz S., Sánchez Román A., Pascual A., Fusco G., Tintoré J. and  
483       Budillon G.: *Monitoring the Algerian Basin through glider observations, satellite altimetry*  
484       *and numerical simulations along a SARAL/AltiKa track*. *Journal of Marine Systems*, 179(),  
485       55–71.[doi:10.1016/j.jmarsys.2017.11.006](https://doi.org/10.1016/j.jmarsys.2017.11.006), 2018

486

487    Aulicino G., Cotroneo Y., Olmedo E., Cesarano C., Fusco G., and Budillon G.: *In Situ and Sat-*  
488       *ellite Sea Surface Salinity in the Algerian Basin Observed through ABACUS Glider Meas-*  
489       *urements and BEC SMOS Regional Products*. *Remote Sensing*, 11(11), 1361–  
490       .[doi:10.3390/rs1111136](https://doi.org/10.3390/rs1111136), 2019.

491

492    Azzaro M., La Ferla R., Maimone G., Monticelli L.S., Zaccone R., and Civitarese G.: *Prokaryotic*  
493       *dynamics and heterotrophic metabolism in a deep convection site of Eastern Mediterranean*  
494       *Sea (the Southern Adriatic Pit)*, *Continental Shelf Research*, Volume 44 2012, Pages 106-118,  
495       ISSN 0278-4343, <https://doi.org/10.1016/j.csr.2011.07.011>, 2012.

496

497    Bensi M., Cardin V., Rubino A., Notarstefano G., and Poulain P.M.: *Effects of winter convection*  
498       *on the deep layer of the Southern Adriatic Sea in 2012*, *J. Geophys. Res. Oceans*  
499       118, 6064– 6075, <https://doi.org/10.1002/2013JC009432>, 2013.

500

501 Bergamasco A., and Malanotte-Rizzoli P.: The circulation of the Mediterranean Sea: A historical  
502 review of experimental investigations. *Adv. Oceanogr. Limnol.* 2010 1 11–28;  
503 <https://doi.org/10.1080/19475721.2010.491656>, 2010.

504

505 Berkowitz J., and Kilian L.: Recent developments in bootstrapping time series. *Econometr Rev*  
506 19:1–48, <https://doi.org/10.1080/07474930008800457>, 2000.

507

508 Borghini M., Bryden H., Schroeder K., Sparnocchia S., and Vetrano A.: The Mediterranean is  
509 becoming saltier, *Ocean Sci.* 10, 693–700, <https://doi.org/10.5194/os-10-693-2014>, 2014.

510

511 Bosse A., Testor P., Mortier L., Prieur L., Taillandier V., d’Ortenzio F., and Coppola L.:  
512 Spreading of Levantine Intermediate Waters by submesoscale coherent vortices in the  
513 northwestern Mediterranean Sea as observed with gliders. *Journal of Geophysical Research.*  
514 *Oceans*, Wiley-Blackwell 2015 120 (3), pp.1599-1622,  
515 <https://doi.org/10.1002/2014JC010263>, 2015.

516

517 Bethoux J.P., Gentili B., Raunet J., and Taillez D.: Warming trend in the Western Mediterranean  
518 deep water. *Nature* 347, 660–662, <https://doi.org/10.1038/347660a0>, 1990.

519

520 Bethoux J. P., Gentili B., Morin P., Nicolas E., Pierre C., and Ruiz-Pino D.: The Mediterranean  
521 Sea: A miniature ocean for climatic and environmental studies and a key for the climatic  
522 functioning of the North Atlantic, *Prog. Oceanogr.*, **44**, 131– 146, doi:[10.1016/S0079-](https://doi.org/10.1016/S0079-6611(99)00023-3)  
523 [6611\(99\)00023-3](https://doi.org/10.1016/S0079-6611(99)00023-3), 1999.

524

525 Cabanes C., Thierry V., and Lagadec C.: Improvement of bias detection in Argo float conductivity  
526 sensors and its application in the North Atlantic. *Deep Sea Research Part I: Oceanographic*  
527 *Research Papers* 114 128-136, <https://doi.org/10.1016/j.dsr.2016.05.007>, 2016.

528

529 Cotroneo Y., Aulicino G., Ruiz S., Pascual A., Budillon G., Fusco G., and Tintoré J.: Glider and  
530 satellite high resolution monitoring of a mesoscale eddy in the algerian basin: Effects on the  
531 mixed layer depth and biochemistry, *Journal of Marine Systems*, Volume 162, Pages 73-88,  
532 ISSN 0924-7963, <https://doi.org/10.1016/j.jmarsys.2015.12.004>, 2016.

533

534 Cotroneo Y., Aulicino G., Ruiz S., Sánchez Román A., Torner Tomàs M., Pascual A., Fusco G.,  
535 Heslop E., Tintoré J., and Budillon G.: Glider data collected during the Algerian Basin Cir-  
536 culation Unmanned Survey, *Earth Syst. Sci. Data*, 11, 147–161, [https://doi.org/10.5194/essd-](https://doi.org/10.5194/essd-11-147-2019)  
537 [11-147-2019](https://doi.org/10.5194/essd-11-147-2019), 2019.

538

539 Demirov E. K., and Pinardi N.: On the relationship between the water mass pathways and eddy  
540 variability in the Western Mediterranean Sea, *J. Geophys. Res.* 112, C02024,  
541 <https://doi.org/10.1029/2005JC003174>, 2007.

542

543 Dickson B., Yashayaev I., Meincke J., Turrell B., Dye S., and Holfort J.: Rapid freshening of the  
544 deep North Atlantic Ocean over the past four decades. *Nature* **416**, 832–837,  
545 <https://doi.org/10.1038/416832a>, 2002.

546

547 Dukhovskoy D.S., Yashayaev I., Proshutinsky A., Bamber J. L., Bashmachnikov I.  
548 L., Chassignet E. P., Lee C.M., and Tedstone A.J.: Role of Greenland freshwater anomaly in  
549 the recent freshening of the subpolar North Atlantic. *Journal of Geophysical Research:*  
550 *Oceans*, 124, 3333– 3360. <https://doi.org/10.1029/2018JC014686>, 2019.

551

552 Escudier R., Mourre B., Juza M., and Tintoré J.: Subsurface circulation and mesoscale variability  
553 in the Algerian subbasin from altimeter-derived eddy trajectories, *J. Geophys.Res. Oceans*  
554 121, 6310–6322, <https://doi.org/10.1002/2016JC011760>, 2016.

555

556 Font J., Millot C., Pérez JDJS, Julià A., and Chic O.: The drift of Modified Atlantic Water from  
557 the Alboran Sea to the eastern Mediterranean. *Scientia Marina*. 62. 211-216,  
558 <https://doi.org/10.3989/scimar.1998.62n3211>, 1998.  
559

560 Giorgi F.: Climate change hot-spots. *Geophysical Research Letters*, 33: L08707,  
561 <https://doi.org/10.1029/2006GL025734>, 2006.  
562

563 Hayes D. R., Schroeder K., Poulain P.M., Testor P., Mortier L., Bosse, A., Du Madron X.: Review  
564 of the Circulation and Characteristics of Intermediate Water Masses of the  
565 Mediterranean: Implications for Cold-Water Coral Habitats. In: Orejas C., Jiménez C.  
566 (eds) *Mediterranean Cold-Water Corals: Past, Present and Future*. Coral Reefs of the  
567 World, vol 9. Springer, Cham, [https://doi.org/10.1007/978-3-319-91608-8\\_18](https://doi.org/10.1007/978-3-319-91608-8_18), 2019.  
568

569 Hernández-Molina F., Stow D., Zarikian C., Acton G., Bahr A., Balestra B., Ducassou E., Flood  
570 R., Flores J.A., Furota S., Grunert P., Hodell D., Jiménez-Espejo F., Kim J.K., Krissek L.,  
571 Kuroda J., Li B., Llave E., Lofi J., and Xuan C.: Onset of Mediterranean outflow into the North  
572 Atlantic. *Science*. 344, <https://doi.org/10.1126/science.1251306>, 2014.  
573

574 Juza M., Escudier R., Vargas-Yáñez M., Mourre B., Heslop E., Allen J., and Tintoré J.: Charac-  
575 terization of changes in Western Intermediate water properties enabled by an innovative ge-  
576 ometry-based detection approach. *Journal of Marine Systems* 191, 1–12. doi:  
577 [10.1016/j.jmarsys.2018.11.003](https://doi.org/10.1016/j.jmarsys.2018.11.003), 2019.  
578

579 Kassis D., and Korres G.: Hydrography of the Eastern Mediterranean basin derived from argo  
580 floats profile data, *Deep Sea Research Part II: Topical Studies in Oceanography*, Volume  
581 171, 2020, 104712, ISSN 0967-0645, <https://doi.org/10.1016/j.dsr2.2019.104712>, 2020.  
582

583 Kokkini Z., Mauri M., Gerin R., Poulain P.M., Simoncelli S., and Notarstefano G.: On the salinity  
584 structure in the South Adriatic as derived from float and glider observations in 2013–2016,  
585 Deep Sea Research Part II: Topical Studies in Oceanography, Volume 171 2020 104625, ISSN  
586 0967-0645, <https://doi.org/10.1016/j.dsr2.2019.07.013>, 2019.

587

588 Kreyszig E.: Introductory Mathematical Statistics: Principles and Methods. New York: Wiley,  
589 1970.

590

591 Kubin E., Poulain P.M, Mauri E., Menna M., and Notarstefano G.: Levantine Intermediate and  
592 Levantine Deep Water Formation: An Argo Float Study from 2001 to 2017,  
593 <https://doi.org/10.3390/w11091781>, 2019.

594

595 Lamer P.A., Mauri E., Notarstefano G., and Poulain P.M.: The Levantine Intermediate Water in  
596 the eastern Mediterranean Sea; [http://maos.inogs.it/pub/REPORT\\_LAMER\\_final\\_last.pdf](http://maos.inogs.it/pub/REPORT_LAMER_final_last.pdf),  
597 2019.

598

599 Lascaratos A., Williams R.G., and Tragou E.: A mixed-layer study of the formation of Levantine  
600 intermediate water. Journal of Geophysical Research 98, <https://doi.org/10.1029/93JC00912>,  
601 1993.

602

603 Lipizer M., Partescano E., Rabitti A., Giorgetti A., and Crise A.: Qualified temperature, salinity  
604 and dissolved oxygen climatologies in a changing Adriatic Sea, Ocean Sci., 10, 771–797,  
605 <https://doi.org/10.5194/os-10-771-2014>, 2014.

606

607 Malanotte-Rizzoli P., Manca B., Marullo S., Ribera d'Alcala M., Roether W., Theocharis A.,  
608 Bergamasco A., Budillon G., Sansone E., Civitarese G., Conversano F., Gertman I., Hernt B,  
609 Kress N., Kioroglou S., Kontoyiannis H., Nittis K., Klein B., Lascaratos A., and Kovacevic  
610 V.: The Levantine Intermediate Water Experiment (LIWEX) Group: Levantine basin—A

611 laboratory for multiple water mass formation processes. *Journal of Geophysical Research*. 108.  
612 8101, <https://doi.org/10.1029/2002JC001643>, 2003.

613

614 Margirier F., Testor P., Heslop E., Mallil K., Bosse A., Houpert L., Mortier L., Bouin M.-  
615 N., Coppola L., D’Ortenzio F., de Madron X.D., Mourre B., Prieur L., Raimbault P., and  
616 Taillandier V.: Abrupt warming and salinification of intermediate waters interplays with  
617 decline of deep convection in the Northwestern Mediterranean Sea. *Sci Rep* 10 20923,  
618 <https://doi.org/10.1038/s41598-020-77859-5>, 2020.

619

620 Mauri E., Sitz L., Gerin R., Poulain P.M., Hayes D., and Gildor H.: On the Variability of the  
621 Circulation and Water Mass Properties in the Eastern Levantine Sea between September 2016–  
622 August 2017. *Water* **2019**, *11*, 1741, <https://doi.org/10.3390/w11091741>, 2019.

623

624 Mauri E., Menna M., Garić R., Batistić M., Libralato S., Notarstefano G., Martellucci R., Gerin  
625 R., Pirro A., Hure M., Poulain P-M, 2021. Recent changes of the salinity distribution and  
626 zooplankton community in the South Adriatic Pit, accepted in *OSR5*.

627

628 **Mihanović, H., Vilibić, I., Šepić, J., Matić, F., Ljubešić, Z., Mauri, E., Gerin, R., Notarstefano,**  
629 **and G., Poulain, P.-M: Observation, preconditioning and recurrence of exceptionally high**  
630 **salinities in the Adriatic Sea. *Frontiers in Marine Sciences*, 8, 672210. doi:**  
631 **[10.3389/fmars.2021.672210](https://doi.org/10.3389/fmars.2021.672210), 2021.**

632

633 Millot C., and Taupier-Letage I.: Circulation in the Mediterranean Sea: Updated description and  
634 schemas of the circulation of the water masses in the whole Mediterranean Sea. A. Saliot. *The*



635 Mediterranean Sea, *The Mediterranean Sea (5-K)*, Springer, pp.29-66 2005, *Handbook of*  
636 *Environmental Chemistry*, 9783540314929 9783540250180. [ff10.1007/b107143ff](https://doi.org/10.1007/b107143ff). [ffhal-](https://doi.org/10.1007/b107143ff)  
637 [01191856v1f](https://doi.org/10.1007/b107143ff), <https://doi.org/10.1007/b107143>, 2005.

638

639 Millot C., Candela J., Fuda J.L., and Tber Y.: Large warming and salinification of the  
640 Mediterranean outflow due to changes in its composition. *Deep-Sea Res.* 53, 656–665,  
641 <https://doi.org/10.1016/j.dsr.2005.12.017>, 2006.

642

643 Millot C.: Interannual salinification of the Mediterranean inflow, *Geophys. Res. Lett.*, 34,  
644 L21609, [doi:10.1029/2007GL031179](https://doi.org/10.1029/2007GL031179), 2007.

645

646 Millot C.: Levantine Intermediate Water characteristics: An astounding general  
647 misunderstanding. *Scientia Marina.* 78, <https://doi.org/10.3989/scimar.04045.30H>, 2013.

648

649 Millot C.: Levantine intermediate water characteristics: an astounding general misunderstanding!  
650 (addendum). *Sci. Marina*, 78 165-171, <https://doi.org/10.3989/scimar.04045.30H>, 2014.

651

652 Nof D.: On man-induced variations in the circulation of the Mediterranean Sea. *Tellus* 31, 558–  
653 564, 1979.

654

655 Notarstefano G., and Poulain P. M.: Delayed mode quality control of Argo floats salinity data in  
656 the Tyrrhenian Sea. Technical Report OGS 2008/125 OGA 43 SIRE,  
657 [http://nettuno.ogs.trieste.it/sire/DMQC/dmqc\\_1900593\\_54073\\_V1.pdf](http://nettuno.ogs.trieste.it/sire/DMQC/dmqc_1900593_54073_V1.pdf), 2008.

658

659 Notarstefano G., and Poulain P. M.: Thermohaline variability in the Mediterranean and Black  
660 Seas as observed by Argo floats in 2000-2009. OGS Tech. Rep. OGS 2009/121 OGA 26 SIRE,  
661 72 pp.-171, <http://dx.doi.org/10.3989/scimar.04045.30H>, 2009.

662

663 Notarstefano G., and Poulain P.M.: Delayed mode quality control of Argo salinity data in the  
664 Mediterranean Sea: A regional approach. Technical Report OGS 2013/103 Sez. OCE 40  
665 MAOS, 2013.

666

667 Ozer T., Gertman I., Kress N., Silverman J., and Herut B.: Interannual thermohaline (1979–2014)  
668 and nutrient (2002–2014) dynamics in the Levantine surface and intermediate water masses,  
669 SE Mediterranean Sea. *Global and Planetary Change*, 151, 60–67.  
670 [doi:10.1016/j.gloplacha.2016.04.001](https://doi.org/10.1016/j.gloplacha.2016.04.001), 2017.

671

672 Painter S.C., and Tsimplis M.N.: Temperature and salinity trends in the upper waters of the  
673 Mediterranean Sea as determined from the MEDATLAS dataset, *Continental Shelf Research*,  
674 Volume 23, Issue 16 2003, Pages 1507-1522, ISSN 0278-4343,  
675 <https://doi.org/10.1016/j.csr.2003.08.008>, 2003.

676

677 Poulain P.M., Barbanti R., Font J., Cruzado A., Millot C., Gertman I., Griffa A., Molcard A.,  
678 Rupolo V., Le Bras S., and Petit de la Villeon L.: MedArgo: a drifting profiler program in the  
679 Mediterranean Sea. *Ocean Science*, European Geosciences Union 2007, 3 (3), pp.379- 395.  
680 hal-00331145, <https://doi.org/10.5194/osd-3-1901-2006>, 2007.

681

682 Poulain P.M., Solari M., Notarstefano G., and Rupolo V.: Assessment of the Argo sampling in  
683 the Mediterranean and Black Seas (part II).  
684 [http://maos.inogs.it/pub/2009\\_report\\_task4.4\\_partII.pdf](http://maos.inogs.it/pub/2009_report_task4.4_partII.pdf), 2009.

685

686 Rahmstorf S.: Influence of Mediterranean Outflow on climate, *Eos Trans. AGU*, **79**, 281– 282,  
687 doi:[10.1029/98EO00208](https://doi.org/10.1029/98EO00208), 1998.

688

689 Rahmstorf, S.: Thermohaline Ocean Circulation. In: *Encyclopedia of Quaternary Sciences*, Edited  
690 by S. A. Elias. Elsevier, Amsterdam, [http://www.pik-](http://www.pik-potsdam.de/~stefan/Publications/Book_chapters/rahmstorf_eqs_2006.pdf)  
691 [potsdam.de/~stefan/Publications/Book\\_chapters/rahmstorf\\_eqs\\_2006.pdf](http://www.pik-potsdam.de/~stefan/Publications/Book_chapters/rahmstorf_eqs_2006.pdf), 2006.

692

693 Roemmich D., Johnson G., Riser S., Davis R., Gilson J., Owens W., Garzoli S., Schmid C., and  
694 Mark I.: The Argo Program Observing the Global Ocean with Profiling Floats. *Oceanography*.  
695 **22**, <https://doi.org/10.5670/oceanog.2009.36>, 2009.

696

697 Rohling E.J., and Bryden H.L.: Man induced salinity and temperature increase in the Western  
698 Mediterranean Deep Water. *J. Geophys. Res.* **97** (C7) 11191–11198,  
699 <https://doi.org/10.1029/92JC00767>, 1992.

700

701 Rubino A., Gačić M., Bensi M., Vedrana K., Vlado M., Milena M., Negretti M.E., Sommeria J.,  
702 Zanchettin D., Barreto R.V., Ursella L., Cardin V., Civitarese G., Orlić M., Petelin B., and

703 Siena G.: Experimental evidence of long-term oceanic circulation reversals without wind  
704 influence in the North Ionian Sea. *Sci Rep* **10** 1905 (2020), [https://doi.org/10.1038/s41598-](https://doi.org/10.1038/s41598-020-57862-6)  
705 [020-57862-6](https://doi.org/10.1038/s41598-020-57862-6), 2020.

706

707 Schroeder K., Chiggiato J., Josey S., Borghini M., Aracri S., and Sparnocchia S.: Rapid response  
708 to climate change in a marginal sea. *Scientific Reports*. **7**, [https://doi.org/10.1038/s41598-017-](https://doi.org/10.1038/s41598-017-04455-5)  
709 [04455-5](https://doi.org/10.1038/s41598-017-04455-5), 2017.

710

711 Schroeder K.: Current Systems in the Mediterranean Sea, Editor(s): J. Kirk Cochran, Henry J.  
712 Bokuniewicz, Patricia L. Yager, *Encyclopedia of Ocean Sciences (Third Edition)*, Academic  
713 Press 2019, Pages 219-227, ISBN 9780128130827, [https://doi.org/10.1016/B978-0-12-](https://doi.org/10.1016/B978-0-12-409548-9.11296-5)  
714 [409548-9.11296-5](https://doi.org/10.1016/B978-0-12-409548-9.11296-5), 2019.

715

716 Schuckmann K.V., Traon P.-Y.L., Smith N., Pascual A., Djavidnia S., Gattuso J.-P., Grégoire M.,  
717 Nolan G., Aaboe S., Aguiar E., et al.: Copernicus marine service ocean state report, issue 3. *J.*  
718 *Oper. Oceanogr*, **12**, S1–S123, 2019.

719

720 Shaltout M., and Omstedt A.: Recent sea surface temperature trends and future scenarios for the  
721 Mediterranean Sea, *Oceanologia*, Volume 56, Issue 3 2014, Pages 411-443, ISSN 0078-3234,  
722 <https://doi.org/10.5697/oc.56-3.411>, 2014.

723

724 Skliris N.: Past, Present and Future Patterns of the Thermohaline Circulation and Characteristic  
725 Water Masses of the Mediterranean Sea. In: Goffredo S., Dubinsky Z. (eds) *The*  
726 *Mediterranean Sea*. Springer, Dordrecht, [https://doi.org/10.1007/978-94-007-6704-1\\_3](https://doi.org/10.1007/978-94-007-6704-1_3), 2014.

727

728 Skliris N., Zika J.D., Herold L., Josey S.A., and Marsh R.: Mediterranean sea water budget long-  
729 term trend inferred from salinity observations. *Clim Dyn* **51** 2857–2876 (2018).  
730 <https://doi.org/10.1007/s00382-017-4053-7>, 2018.

731

732 Tsimplis M., Zervakis V., Josey S.A., Peneva E., Struglia M.V., Stanev E., Lionello P.,  
733 Malanotte-Rizzoli P., Artale V., Theocharis A., Tragou E., and Oguz T.: Changes in the  
734 oceanography of the Mediterranean Sea and their link to climate variability. In: Lionello, P.;  
735 Malanotte-Rizzoli, P.; and Boscolo, R., (eds.) Mediterranean climate variability. Amsterdam,  
736 The Netherlands, Elsevier 227-282, 438pp. (Developments in Earth and Environmental  
737 Sciences, 4), [https://doi.org/10.1016/S1571-9197\(06\)80007-8](https://doi.org/10.1016/S1571-9197(06)80007-8), 2006.

738

739 Vàrgas-Yáñez M., Moya F., Tel E., García-Martínez M.C., Guerber E., and Bourgeon M.:  
740 Warming and salting of the Western Mediterranean during the second half of the XX century:  
741 inconsistencies, unknowns and the effect of data processing. Sci. Mar. 73 (1), 7–28,  
742 <https://doi.org/10.3989/scimar.2009.73n1007>, 2009.

743

744 Vàrgas-Yáñez M., Moya F., García-Martínez M.C., Tel E., Zunino P., Plaza F., Salat J., Pascual  
745 J., López-Jurado J.L., and Serra M.: Climate change in the Western Mediterranean Sea 1900–  
746 2008, Journal of Marine Systems, Volume 82, Issue 3 2010, Pages 171-176, ISSN 0924-7963,  
747 <https://doi.org/10.1016/j.jmarsys.2010.04.013>, 2010.

748

749 Vàrgas-Yáñez M., Juza M., Balbín R., Velez-Belchí P., García-Martínez M. C., Moya F., and  
750 Hernández-Guerra A.: Climatological Hydrographic Properties and Water Mass Transports in  
751 the Balearic Channels From Repeated Observations Over 1996–2019, Frontiers in Marine  
752 Science, Volume 7, Pages 779, IISN 2296-7745,  
753 <https://www.frontiersin.org/article/10.3389/fmars.2020.568602>, 2020.

754

755 Vilibić, I., Matijević, S., Šepić, J., and Kušpilić G.: Changes in the Adriatic oceanographic  
756 properties induced by the Eastern Mediterranean Transient, Biogeosciences, 9, 2085–2097,  
757 <https://doi.org/10.5194/bg-9-2085-2012>, 2012.

758 Vilibić, I., Šepić, J., and Proust, N.: Weakening of thermohaline circulation in the Adriatic Sea.  
759 *Climate Research*, 55, 217–225, 2013.

760

761 Vilibić, I., Zemunik, P., Dunić, N., and Mihanović, H.: Local and remote drivers of the observed  
762 thermohaline variability on the northern Adriatic shelf (Mediterranean Sea). *Cont. Shelf Res.*  
763 199:104110. doi: 10.1016/j.csr.2020.104110, 2020.

764

765 Wong A., Keeley R., Carval T., Argo Data Management Team: Argo Quality Control Manual for  
766 CTD and Trajectory Data, <https://doi.org/10.13155/33951>, 2021.

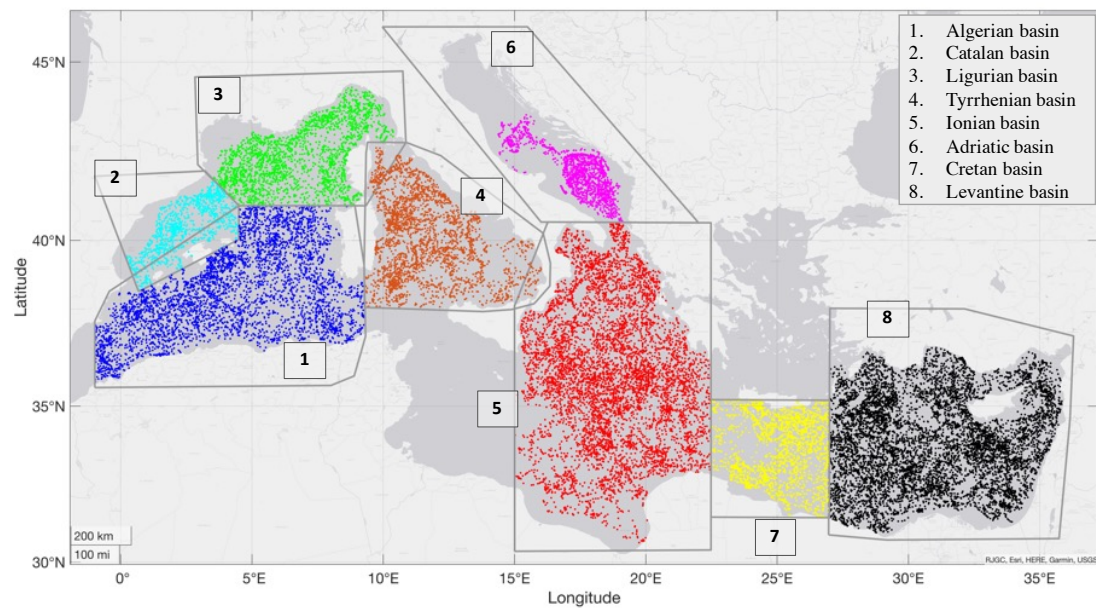
767

768 Zu Z., Poulain P.M., and Notarstefano G.: Changes in hydrological properties of the  
769 Mediterranean Sea over the last 40 years with focus on the Levantine Intermediate Water and  
770 the Atlantic Water, [http://maos.inogs.it/pub/Hydro\\_trend\\_LIW\\_SAW\\_core\\_report\\_v10.pdf](http://maos.inogs.it/pub/Hydro_trend_LIW_SAW_core_report_v10.pdf),  
771 2014.

772

**Table 1.** Trends by year for the AW and LIW salinity, temperature, and depth timeseries in eight Mediterranean subbasins. In bold characters the trends significant at 5% level. The rightmost column shows the mean and standard deviation trend values computed over the eight subbasins (here identified with MED). Trends are defined as mean  $\pm$  standard deviation.

|                            | Algerian                           | Catalan                            | Ligurian                          | Tyrrhenian                          | Adriatic                          | Ionian                              | Cretan                              | Levantine                          | MED                                |
|----------------------------|------------------------------------|------------------------------------|-----------------------------------|-------------------------------------|-----------------------------------|-------------------------------------|-------------------------------------|------------------------------------|------------------------------------|
| <b>Salinity [1/yr]</b>     |                                    |                                    |                                   |                                     |                                   |                                     |                                     |                                    |                                    |
| AW                         | <b>-0.014<math>\pm</math>0.151</b> | <b>-0.004<math>\pm</math>0.088</b> | -0.001 $\pm$ 0.089                | <b>0.006<math>\pm</math>0.157</b>   | <b>0.044<math>\pm</math>0.188</b> | <b>0.009<math>\pm</math>0.181</b>   | <b>0.013<math>\pm</math>0.166</b>   | <b>0.003<math>\pm</math>0.100</b>  | <b>0.007<math>\pm</math>0.140</b>  |
| LIW                        | <b>0.002<math>\pm</math>0.022</b>  | <b>0.002<math>\pm</math>0.017</b>  | <b>0.005<math>\pm</math>0.034</b> | <b>0.006<math>\pm</math>0.035</b>   | <b>0.021<math>\pm</math>0.074</b> | <b>0.004<math>\pm</math>0.031</b>   | <b>0.005<math>\pm</math>0.048</b>   | <b>0.004<math>\pm</math>0.039</b>  | <b>0.006<math>\pm</math>0.038</b>  |
| <b>Temperature [°C/yr]</b> |                                    |                                    |                                   |                                     |                                   |                                     |                                     |                                    |                                    |
| AW                         | <b>0.054<math>\pm</math>0.614</b>  | 0.019 $\pm$ 0.846                  | 0.004 $\pm$ 0.914                 | <b>0.042<math>\pm</math>0.528</b>   | <b>0.117<math>\pm</math>0.951</b> | <b>0.023<math>\pm</math>0.395</b>   | <b>-0.026<math>\pm</math>0.786</b>  | <b>0.026<math>\pm</math>0.683</b>  | <b>0.026<math>\pm</math>0.715</b>  |
| LIW                        | <b>0.008<math>\pm</math>0.125</b>  | <b>0.010<math>\pm</math>0.088</b>  | <b>0.022<math>\pm</math>0.138</b> | <b>0.030<math>\pm</math>0.167</b>   | <b>0.093<math>\pm</math>0.384</b> | <b>0.030<math>\pm</math>0.226</b>   | -0.003 $\pm$ 0.226                  | <b>0.012<math>\pm</math>0.391</b>  | <b>0.022<math>\pm</math>0.232</b>  |
| <b>Depth [m/yr]</b>        |                                    |                                    |                                   |                                     |                                   |                                     |                                     |                                    |                                    |
| AW                         | <b>-0.092<math>\pm</math>2.271</b> | -0.019 $\pm$ 4.646                 | -0.012 $\pm$ 5.720                | <b>0.394<math>\pm</math>4.002</b>   | 0.757 $\pm$ 25.800                | <b>-0.324<math>\pm</math>7.352</b>  | 0.116 $\pm$ 17.480                  | <b>1.087<math>\pm</math>17.024</b> | <b>0.238<math>\pm</math>10.537</b> |
| LIW                        | -0.352 $\pm$ 14.639                | <b>1.895<math>\pm</math>52.582</b> | -0.155 $\pm$ 40.249               | <b>-7.034<math>\pm</math>46.395</b> | 2.609 $\pm$ 115.404               | <b>-4.973<math>\pm</math>42.536</b> | <b>-1.630<math>\pm</math>26.943</b> | <b>0.849<math>\pm</math>32.912</b> | <b>1.099<math>\pm</math>46.458</b> |

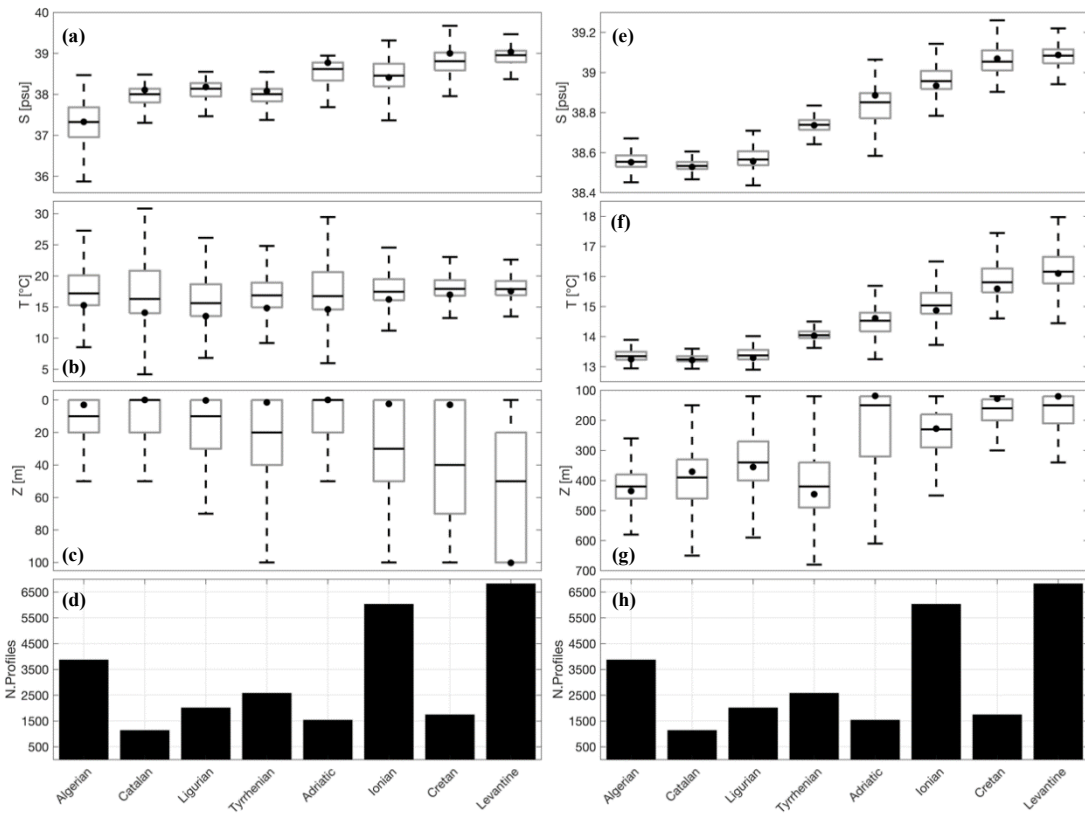


775

776 Fig. 1 Argo floats profiles scatter plot in the Mediterranean Sea between 2001 and 2019 in eight

777 regions based on the climatological areas defined by the EU/MEDARMEDATLAS II project.

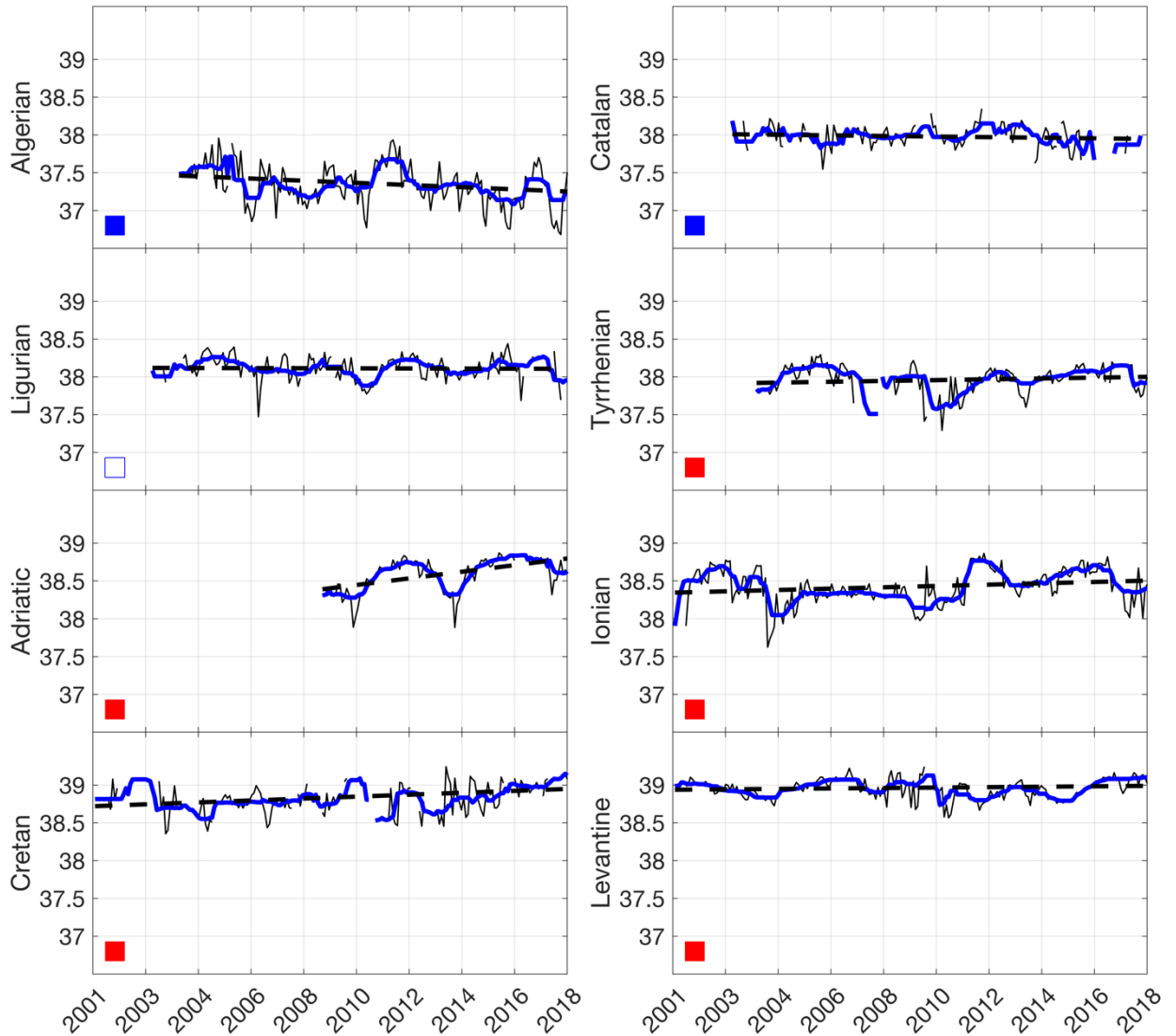




778

779 Fig. 2 Boxplot diagrams for the AW salinity (a), temperature (b) and depth (c) in eight  
 780 Mediterranean subbasins. Inside each grey box, the black bold line indicates the median, while  
 781 the bottom and top edges of the box indicate the 25th and 75th percentiles respectively, and the  
 782 black dots show the mode of each distribution, which corresponds to the maximum PDF. The  
 783 number of profiles (black bars) for each subbasin are shown in panel (d). The corresponding  
 784 diagrams for the LIW are shown in the panels (e,f,g,h).

### Salinity [psu]



785

786 Fig. 3 AW salinity timeseries in eight subbasins: the thin black lines show the monthly timeseries

787 (seasonal cycle filtered out), the thick blue lines are the 1-year moving average timeseries and the

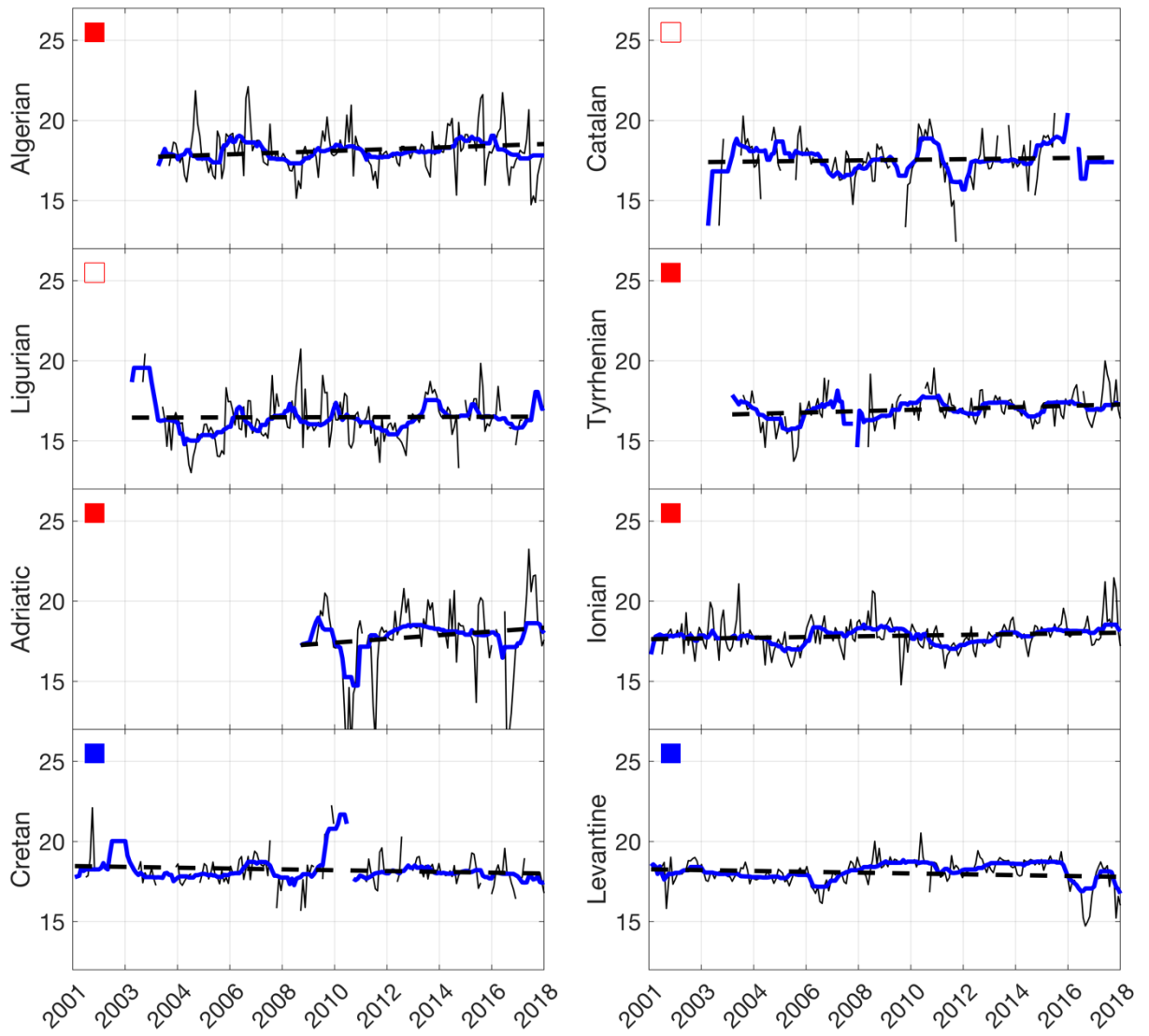
788 dashed black lines are the trends. The red/blue filled squares identify the positive/negative trends

789 with  $pvalue \leq 0.05$ , while the red/blue not-filled squares identify the positive/negative trends with

790  $pvalue > 0.05$ .

791

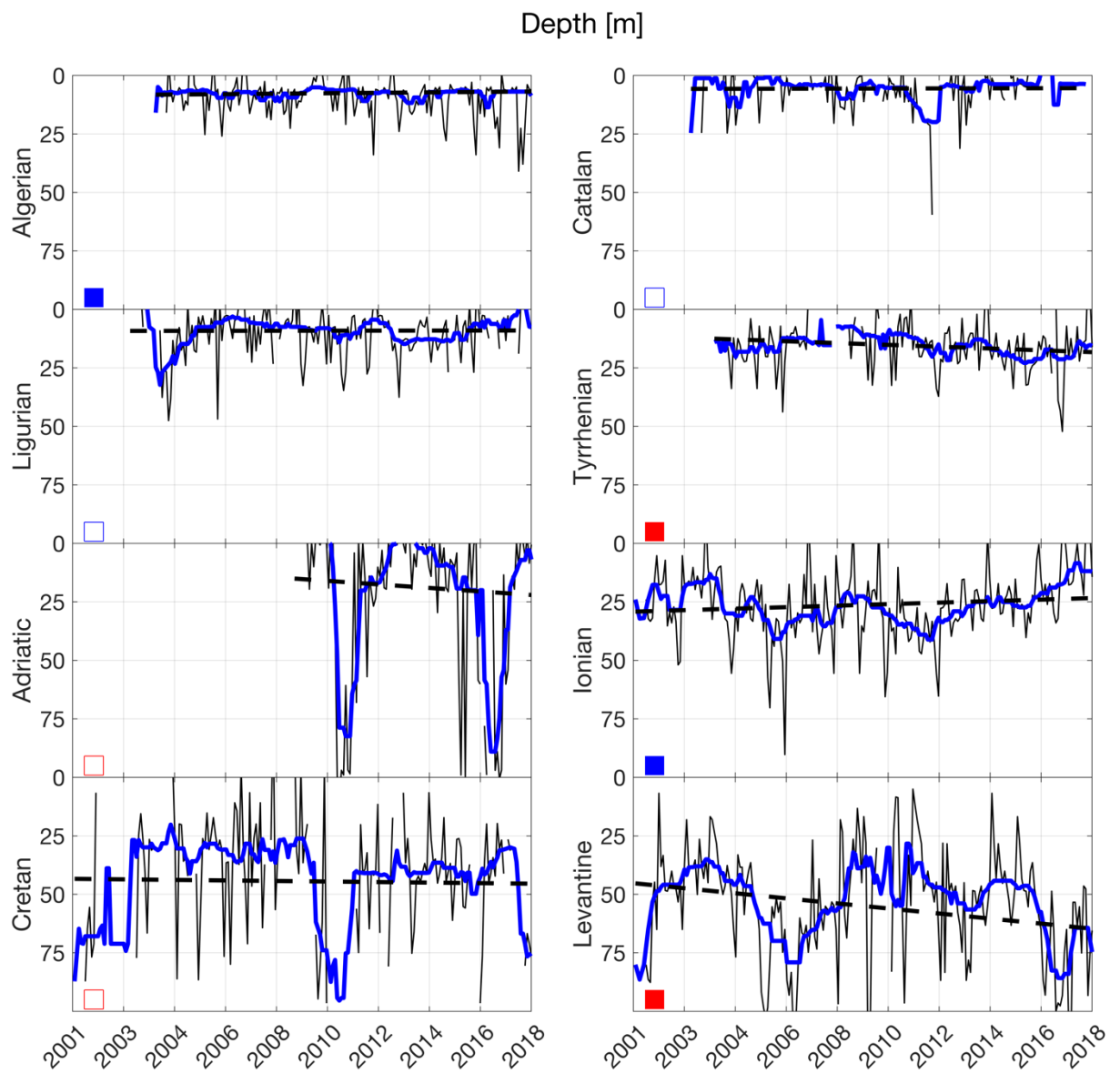
Temperature [°C]



792

793 Fig. 4 Same as Fig. 3 but for the AW temperature.

794



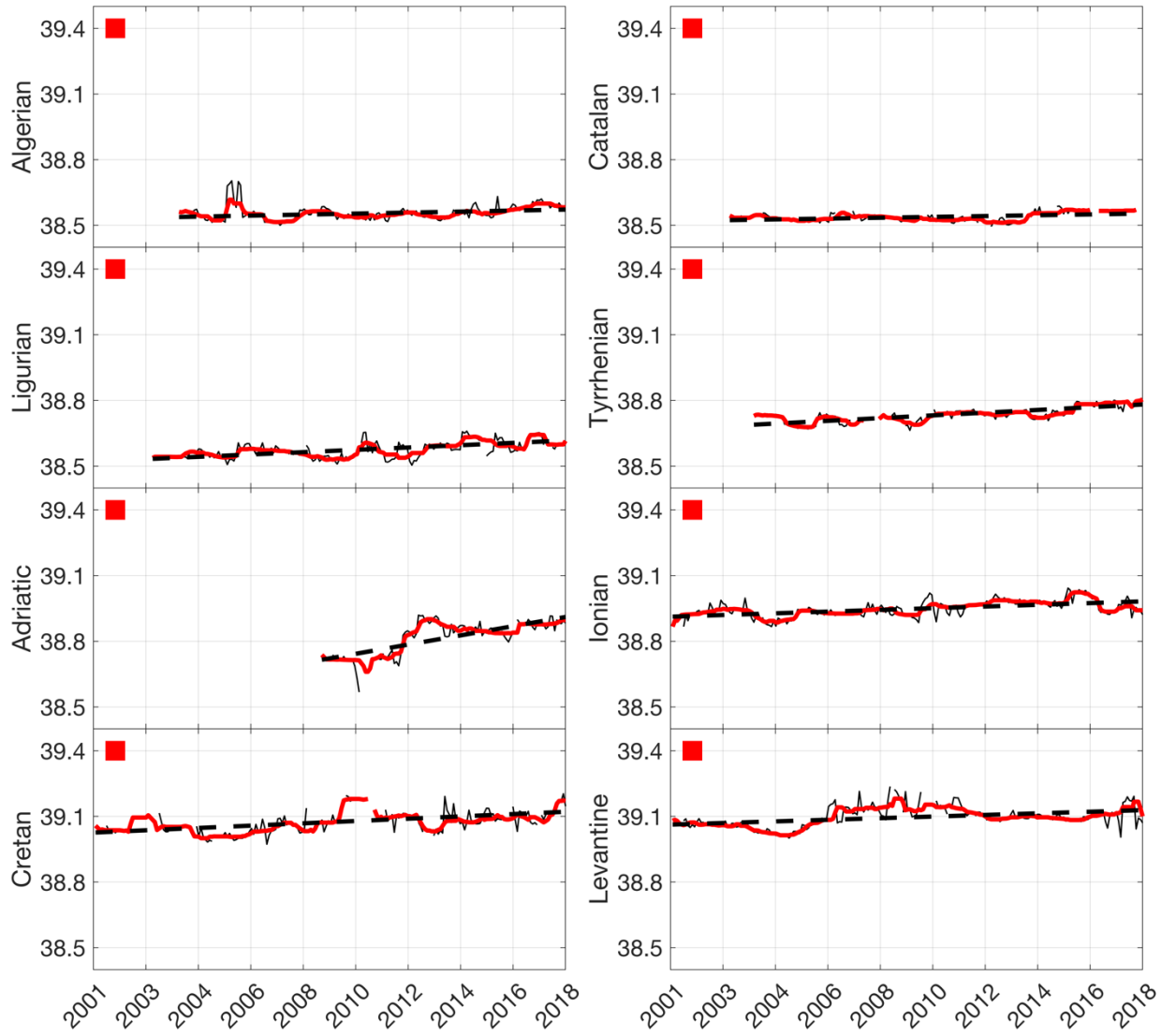
795

796 Fig. 5 Same as Fig. 3 but for the AW depth. Positive/negative trends (red/blue squares) in this

797 case corresponds to an increase/decrease of the depth (i.e., deeper/shallower).

798

Salinity [psu]

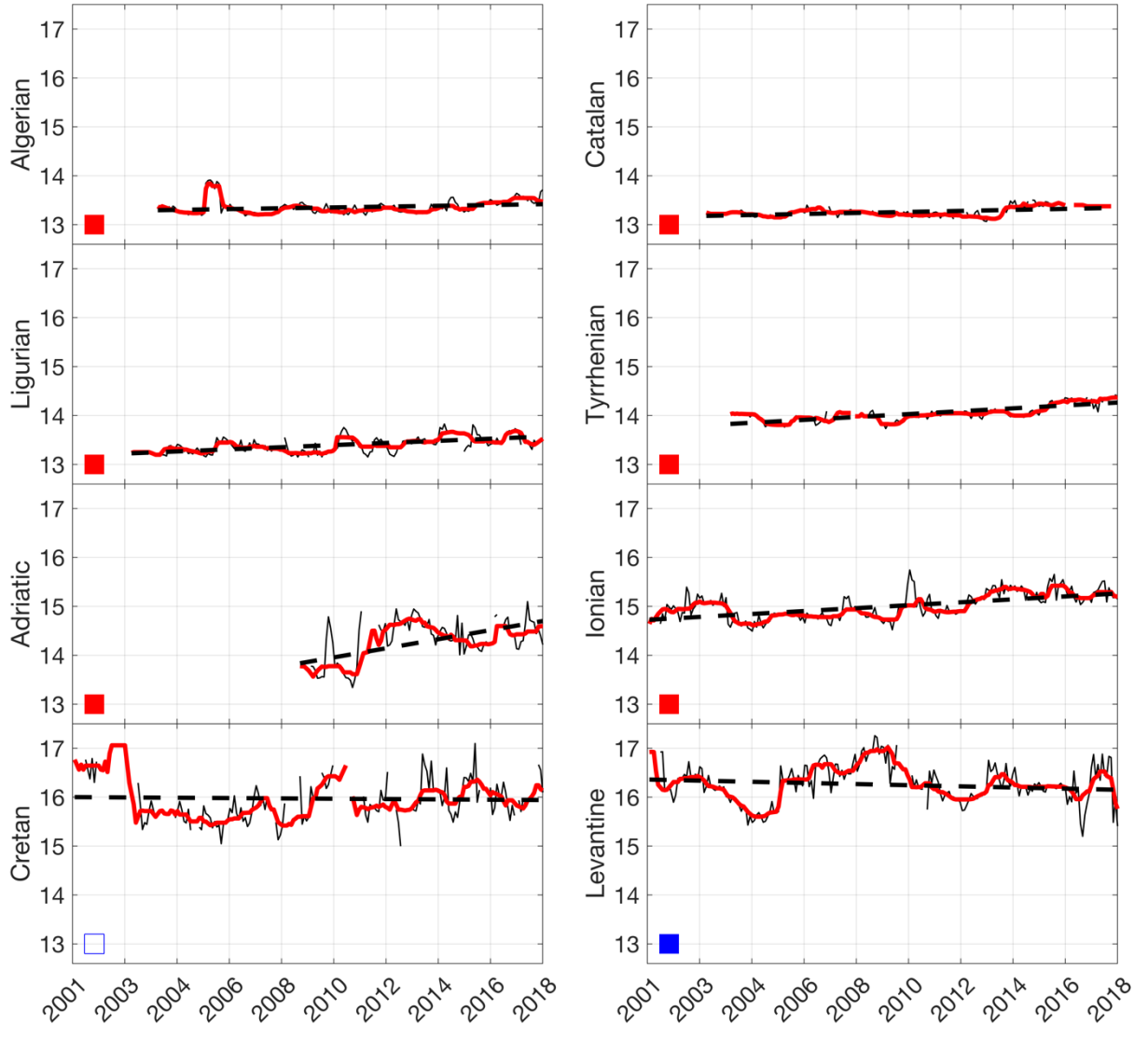


799

800 Fig. 6 Same as Fig. 3 but for the LIW salinity.

801

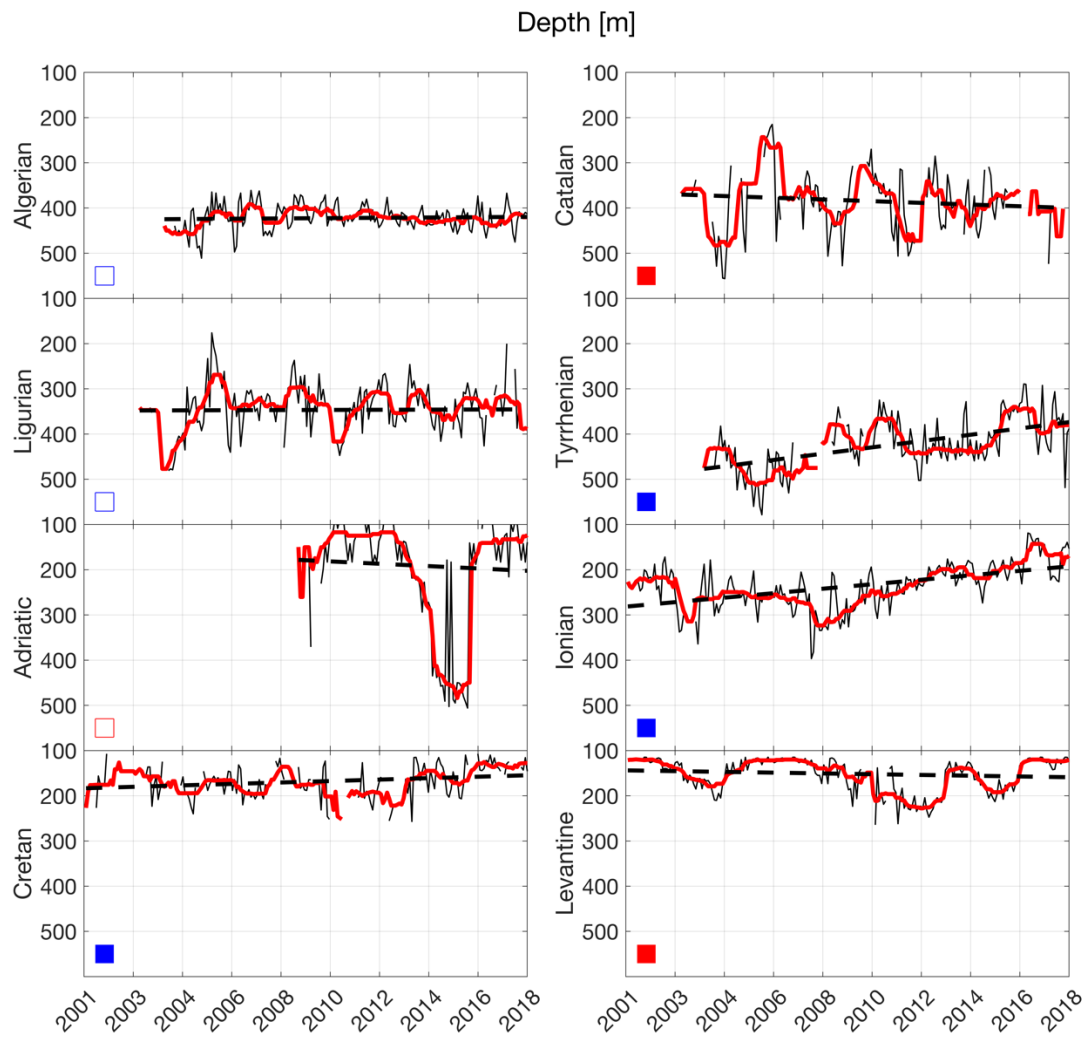
Temperature [°C]



802

803 Fig. 7 Same as Fig. 3 but for the LIW temperature.

804



805

806 Fig. 8 Same as Fig. 3 but for the LIW depth. Positive/negative trends (red/blue squares) in this

807 case corresponds to an increase/decrease of the depth (i.e., deeper/shallower).